



Global  
measurements of  
HCN and C<sub>2</sub>H<sub>2</sub> from  
IASI

V. Dufлот et al.

This discussion paper is/has been under review for the journal Atmospheric Chemistry and Physics (ACP). Please refer to the corresponding final paper in ACP if available.

# Acetylene (C<sub>2</sub>H<sub>2</sub>) and hydrogen cyanide (HCN) from IASI satellite observations: global distributions, validation, and comparison with model

V. Dufлот<sup>1,2</sup>, C. Wespes<sup>1</sup>, L. Clarisse<sup>1</sup>, D. Hurtmans<sup>1</sup>, Y. Ngadi<sup>1</sup>, N. Jones<sup>3</sup>, C. Paton-Walsh<sup>3</sup>, J. Hadji-Lazaro<sup>4</sup>, C. Vigouroux<sup>5</sup>, M. De Mazière<sup>5</sup>, J.-M. Metzger<sup>6</sup>, E. Mahieu<sup>7</sup>, C. Servais<sup>7</sup>, F. Hase<sup>8</sup>, M. Schneider<sup>8</sup>, C. Clerbaux<sup>1,4</sup>, and P.-F. Coheur<sup>1</sup>

<sup>1</sup>Spectroscopie de l'Atmosphère, Service de Chimie Quantique et Photophysique, Université Libre de Bruxelles (U.L.B.), 50 Av. F. D. Roosevelt, 1050, Brussels, Belgium

<sup>2</sup>Laboratoire de l'Atmosphère et des Cyclones (LACy), Université de la Réunion, UMR CNRS-Météo-France 8105, Saint-Denis de la Réunion, France

<sup>3</sup>School of Chemistry, University of Wollongong, Wollongong, New South Wales, Australia

<sup>4</sup>UPMC Université Paris 06; Université Versailles-St. Quentin; CNRS/INSU, LATMOS-IPSL, Paris, France

<sup>5</sup>Belgian Institute for Space Aeronomy (BIRA-IASB), 3, Av. Circulaire, 1180, Brussels, Belgium

Title Page

Abstract

Introduction

Conclusions

References

Tables

Figures



Back

Close

Full Screen / Esc

Printer-friendly Version

Interactive Discussion



<sup>6</sup>UMS3365 de l'OSU-Réunion, CNRS – Université de la Réunion, Saint Denis de la Réunion, France

<sup>7</sup>Institut d'Astrophysique et de Géophysique, Université de Liège, 17, Allée du 6 Août, 4000, Liège, Belgium

<sup>8</sup>Institute for Meteorology and Climate Research (IMK-ASF), Karlsruhe Institute of Technology, Karlsruhe, Germany.

Received: 13 April 2015 – Accepted: 20 April 2015 – Published: 21 May 2015

Correspondence to: V. Dufлот (valentin.dufлот@univ-reunion.fr)

Published by Copernicus Publications on behalf of the European Geosciences Union.

Global  
measurements of  
HCN and C<sub>2</sub>H<sub>2</sub> from  
IASI

V. Dufлот et al.

Title Page

Abstract

Introduction

Conclusions

References

Tables

Figures



Back

Close

Full Screen / Esc

Printer-friendly Version

Interactive Discussion



## Abstract

We present global distributions of  $C_2H_2$  and HCN total columns derived from the Infrared Atmospheric Sounding Interferometer (IASI). These distributions are obtained with a fast method allowing to retrieve  $C_2H_2$  abundance globally with a 5% precision and HCN abundance in the tropical (subtropical) belt with a 10% (30%) precision. IASI data are compared for validation purposes with ground-based Fourier Transform Infrared (FTIR) spectrometer measurements at four selected stations. We show that there is an overall agreement between the ground-based and space measurements. Global  $C_2H_2$  and subtropical HCN abundances retrieved from IASI spectra show the expected seasonality linked to variations in the anthropogenic emissions and seasonal biomass burning activity, as well as exceptional events, and are in good agreement with previous spaceborne studies. IASI measurements are also compared to the distributions from the Model for Ozone and Related Chemical Tracers, version 4 (MOZART-4). Seasonal cycles observed from satellite data are reasonably well reproduced by the model. However, the model seems to overestimate (underestimate) anthropogenic (biomass burning) emissions and a negative global mean bias of 1% (16%) of the model relative to the satellite observations was found for  $C_2H_2$  (HCN).

## 1 Introduction

Hydrogen cyanide (HCN) and acetylene (or ethyne,  $C_2H_2$ ) are ubiquitous atmospheric trace gases with medium lifetime, which are frequently used as indicators of combustion sources and as tracers for atmospheric transport and chemistry. For HCN, biomass burning is the primary source, followed by fossil fuel combustion and higher plants, bacteria and fungi (Cicerone and Zellner, 1983; Li et al., 2000), and its primary sink is thought to be ocean uptake (Li et al., 2000). For  $C_2H_2$ , biofuel combustion is considered as the dominant source, followed by fossil fuel combustion and biomass burning

ACPD

15, 14357–14401, 2015

### Global measurements of HCN and $C_2H_2$ from IASI

V. Dufлот et al.

Title Page

Abstract

Introduction

Conclusions

References

Tables

Figures

◀

▶

◀

▶

Back

Close

Full Screen / Esc

Printer-friendly Version

Interactive Discussion







## Global measurements of HCN and C<sub>2</sub>H<sub>2</sub> from IASI

V. Duflot et al.

Title Page

Abstract

Introduction

Conclusions

References

Tables

Figures



Back

Close

Full Screen / Esc

Printer-friendly Version

Interactive Discussion



*Atmosphit* (Coheur et al., 2005). In the cases of HCN and C<sub>2</sub>H<sub>2</sub>, the accuracy of the retrievals has been recently improved by taking into consideration the CO<sub>2</sub> line mixing in the radiative transfer model (Duflot et al., 2013). This retrieval method, relying on spectral fitting, needs a high computational power and is time consuming, especially when a large number of spectra has to be analyzed and fitted. This is therefore not suitable for providing global scale concentrations distributions of these trace gases in a reasonable time.

One of the commonly used methods for the fast detection of trace gases is the brightness temperature difference (BTD) between a small number of channels, some being sensitive to the target species, some being not. Such a method has been used from IASI spectra for sulfur dioxide (SO<sub>2</sub>) (Clarisse et al., 2008) and ammonia (NH<sub>3</sub>) (Clarisse et al., 2009). It is of particular interest in operational applications (quick alerts) or when large amounts of data need to be processed. However, relying on a cautious selection of channels to avoid the contamination with other trace gases, the BTD method does not fully exploit all the information contained in hyperspectral measurements. Especially, low concentrations of the target species may not be detected with such a method.

Walker et al. (2011) presented a fast and reliable method for the detection of atmospheric trace gases that fully exploits the spectral range and spectral resolution of hyperspectral instruments in a single retrieval step. They used it to retrieve SO<sub>2</sub> total column from a volcanic plume and NH<sub>3</sub> total column above India. More recently, Van Damme et al. (2014) presented a retrieval scheme to retrieve NH<sub>3</sub> from IASI spectra based on the work of Walker et al. (2011), and introduced a metric called Hyperspectral Range Index (HRI). We use in the present study a similar approach.

### 2.2.1 Hyperspectral Range Index (HRI)

The method used in this study is a non-iterative pseudo retrieval method of a single physical variable or target species  $x$  expressed as, following the formalism developed







## Global measurements of HCN and C<sub>2</sub>H<sub>2</sub> from IASI

V. Dufлот et al.

Title Page

Abstract

Introduction

Conclusions

References

Tables

Figures

◀

▶

◀

▶

Back

Close

Full Screen / Esc

Printer-friendly Version

Interactive Discussion



in Sect. 2.2.3). Each of the constructed profile has been associated with a spectrum through the FM of *Atmosphit* considering standard absorption profiles. The associated values of  $\text{HRI}_{\text{HCN}}$  and  $\text{HRI}_{\text{C}_2\text{H}_2}$  have then been computed for each of the simulated spectra. Figure 2 shows the look up tables (LUTs) of  $\text{HRI}_{\text{HCN}}$  (top) and  $\text{HRI}_{\text{C}_2\text{H}_2}$  (bottom) as a function of the abundance of the target molecule and of the altitude of the polluted layer in a standard tropical modeled atmosphere (Anderson et al., 1986). Similar LUTs have been computed for standard temperate (US standard atmosphere) and polar (Anderson et al., 1986) atmospheres (data not shown). The satellite viewing angles were taken into account in the HRI calculation similarly to Van Damme et al. (2014). One can see that, for a given atmosphere and for a given altitude of the polluted layer, the abundances of both species linearly depend on the HRI value, which validates Eq. (5). For a given atmosphere atm and a given species  $X$ , the different values of  $B$  with respect to the altitude  $z$  of the polluted layer will be noted  $b_{X_{\text{atm}}}(z)$  and  $k_{X_{\text{atm}}}(z)$  in the following.

Figure 3 shows the normalised Jacobians of the FM for HCN and C<sub>2</sub>H<sub>2</sub> averaged over the spectral ranges given in Sect. 2.2.1 (645–800 cm<sup>-1</sup> for HCN and 645–845 cm<sup>-1</sup> for C<sub>2</sub>H<sub>2</sub>) and for each of the three standard modeled atmospheres. These Jacobians express the sensitivity of the FM, i.e. both the radiative transfer model and IASI (through its instrumental function), to the target species abundance  $X$  in a fixed atmosphere atm:

$$K_{X_{\text{atm}}} = \left[ \frac{\partial F_{\text{atm}}}{\partial X}(z_1) \dots \frac{\partial F_{\text{atm}}}{\partial X}(z_n) \right] = \left[ k_{X_{\text{atm}}}(z_1) \dots k_{X_{\text{atm}}}(z_n) \right] \quad (6)$$

We then obtain the coefficients  $B_{X_{\text{atm}}}$  by multiplying the  $b_{X_{\text{atm}}}(z)$  by the value of the Jacobian at the altitude  $z$ :

$$B_{X_{\text{atm}}} = \sum_{i=1}^n \left( b_{X_{\text{atm}}}(z_i) \times k_{X_{\text{atm}}}(z_i) \right) \quad \text{with} \quad \sum_{i=1}^n k_{X_{\text{atm}}}(z_i) = 1 \quad (7)$$

Applying this method to the three standard modeled atmospheres (tropical, temperate and polar), we get a  $B_X$  value for each, which we have associated with the corresponding range of latitude ( $[\pm 20^\circ]$ ,  $[\pm 45^\circ : \pm 60^\circ]$ ,  $[\pm 75^\circ : \pm 90^\circ]$ , respectively), and linearly interpolated between. Figure 4 gives the resulting values of  $B_{\text{HCN}}$  (blue) and  $B_{\text{C}_2\text{H}_2}$  (green) in function of the latitude.

### 2.2.3 Sensitivity and stability of the method

The sensitivity of the method can be assessed from the Jacobians presented in Fig. 3. For HCN, one can see that there is no sensitivity at the surface and above  $\sim 30$  km, and the altitude of the sensitivity peak is located close to the tropopause at  $\sim 9$ ,  $\sim 11$  and  $\sim 14$  km for the polar, temperate and tropical atmospheres, respectively. For  $\text{C}_2\text{H}_2$ , there is no sensitivity above  $\sim 20$  km, and the maximum sensitivity is reached at  $\sim 8$ ,  $\sim 10$  and  $\sim 11$  km for the polar, temperate and tropical atmospheres, respectively.

The HRIs presented here above are sensitive to the abundance of the target species – this is what they are made for – and to their vertical distribution. However, the measured column amount may also depend on: (1) the proper suppression of the spectral background, (2) the conditions of thermal contrast with the surface (TC), and (3) the accuracy of the FM to simulate the spectra used to build up the LUTs. The latter was discussed already by Dufлот et al. (2013). In order to test the impact of the two first factors (spectral background suppression and TC) on the retrieved column amount, HCN and  $\text{C}_2\text{H}_2$  profiles have been constructed with varying TC and concentrations of the interfering and target species. The TC is defined here as the difference between the skin (surface) temperature and that of the air at an altitude of 1.5 km. These variations in interfering species abundances and TC were considered to be independent and were taken within the range  $\pm 2\%$  for  $\text{CO}_2$  and  $\pm 20\%$  for  $\text{H}_2\text{O}$  and  $\text{O}_3$ , and in the range  $\pm 10\text{K}$  for the TC. For a fixed column amount of the target species, the HRIs were compared one by one to a HRI corresponding to a standard spectrum (i.e. with background concentrations of the interfering species and a TC equal to zero) and if the

## Global measurements of HCN and $\text{C}_2\text{H}_2$ from IASI

V. Dufлот et al.

Title Page

Abstract

Introduction

Conclusions

References

Tables

Figures

◀

▶

◀

▶

Back

Close

Full Screen / Esc

Printer-friendly Version

Interactive Discussion





### 3 Results

The goal of this section is to describe and evaluate the C<sub>2</sub>H<sub>2</sub> and HCN total columns as measured by IASI. We first compare HCN and C<sub>2</sub>H<sub>2</sub> total columns retrieved from IASI spectra and from ground-based FTIR spectra. We then depict the C<sub>2</sub>H<sub>2</sub> and HCN total columns at global and regional scales. IASI global and regional distributions are finally compared with output from the Model for Ozone and Related Chemical Tracers, version 4 (MOZART-4) in order to evaluate the agreement between the model and the IASI distributions.

#### 3.1 Comparison with ground-based observations

We compare in this section HCN and C<sub>2</sub>H<sub>2</sub> total columns retrieved from IASI spectra and from ground-based FTIR spectra for the years 2008–2010 for four selected ground-based FTIR observation sites: Wollongong (34° S; 151° E; 30 m a.m.s.l.), Reunion Island (21° S; 55° E; 50 m a.m.s.l.), Izaña (28° N; 16° W; 2367 m a.m.s.l.) and Jungfrau-joch (46° N; 8° E; 3580 m a.m.s.l.) (Fig. 6). IASI cloudy spectra were removed from the data set using a 10 % contamination threshold on the cloud fraction in the pixel. As exposed in Sect. 2.2.3, errors in retrieved species abundances from IASI spectra due to variations in atmospheric parameters are 10 % at tropical latitudes ([±20°]) and 30 % at subtropical latitudes ([±35° : ±20°]) for HCN and 5 % for C<sub>2</sub>H<sub>2</sub>, and comparison with ground-based HCN measurements are only performed for tropical and subtropical sites (Reunion Island, Wollongong and Izaña).

Total errors for ground-based measurements at Reunion Island are 17 % for both species, total error for HCN ground-based measurements at Wollongong is 15 %, total error for HCN ground-based measurements at Izaña is 10 %, and total error for C<sub>2</sub>H<sub>2</sub> ground-based measurements at Jungfrau-joch is 7 %. Detailed description of ground-based FTIR data set, retrieval method and error budget can be found in Vigouroux et al. (2012) for Reunion Island and in Mahieu et al. (2008) for Jungfrau-joch. However, at Reunion Island, the retrieval strategies have been slightly improved from Vigouroux

Title Page

Abstract

Introduction

Conclusions

References

Tables

Figures



Back

Close

Full Screen / Esc

Printer-friendly Version

Interactive Discussion



et al. (2012), mainly concerning the treatment of the interfering species, but the same spectral signatures are used. Izaña data set and error budget were obtained from the NDACC database (<ftp://ftp.cpc.ncep.noaa.gov/ndacc/station/izana/>). Wollongong data set and error budget were calculated by N. Jones from the University of Wollongong (N. Jones, personal communication, 2015).

Figure 7 shows the mean total column averaging kernels for the ground-based FTIR at each of the four sites. Similarly to IASI (Fig. 3), information content from ground-based instruments measurements is mostly in the middle-high troposphere for both species. The main difference can be observed for tropical  $C_2H_2$ : while IASI Jacobian peaks at 10 km for  $C_2H_2$  in a tropical atmosphere, ground-based FTIR averaging kernel peaks at 15 km for  $C_2H_2$  at Reunion Island.

Figure 8 shows the comparison between the IASI and the ground-based measurements. IASI retrieved total columns were averaged on a daily basis and on a  $1^\circ \times 1^\circ$  area around the observation sites. HCN retrieved abundances below  $2.8 \times 10^{15}$  molec  $cm^{-2}$  have been removed from both ground-based and space measurements to allow comparison of both datasets (cf. Sect. 2.2.3). One can see that there is an overall agreement between the IASI and the ground-based FTIR measurements considering the error bars. An important result from this study is that IASI seems to capture the seasonality in the two species in most of the cases. This is best seen by looking at the IASI monthly mean retrieved total columns (black circles and lines in Fig. 8). The scatter of the IASI daily mean measurements (red dots) are due to the averaging on a  $1^\circ \times 1^\circ$  area around the observation sites.

At Reunion Island HCN and  $C_2H_2$  peak in October-November and are related to the Southern Hemisphere biomass burning season (Vigouroux et al., 2012). We find maxima of around  $12 \times 10^{15}$  molec  $cm^{-2}$  for HCN and  $10 \times 10^{15}$  molec  $cm^{-2}$  for  $C_2H_2$ . The seasonality and interannual variability matches very well that of the ground-based FTIR measurements for HCN (correlation coefficient of 0.81 for the entire daily mean dataset, and of 0.98 for the monthly mean data set) but with the IASI columns being biased high by  $0.79 \times 10^{15}$  molec  $cm^{-2}$  (17%). For  $C_2H_2$  at Reunion Island, the sea-

## Global measurements of HCN and $C_2H_2$ from IASI

V. Dufлот et al.

Title Page

Abstract

Introduction

Conclusions

References

Tables

Figures

◀

▶

◀

▶

Back

Close

Full Screen / Esc

Printer-friendly Version

Interactive Discussion



**Global  
measurements of  
HCN and C<sub>2</sub>H<sub>2</sub> from  
IASI**

V. Duflot et al.

Title Page

Abstract

Introduction

Conclusions

References

Tables

Figures



Back

Close

Full Screen / Esc

Printer-friendly Version

Interactive Discussion



sonality and interannual variability matches reasonably well that of the ground-based measurements (correlation coefficient of 0.40 for the entire daily mean dataset, and of 0.72 for the monthly mean data set) but with the IASI columns being biased high by  $1.10 \times 10^{15} \text{ molec cm}^{-2}$  (107%). Such a high bias between the two datasets could be due to the difference between space and ground-based instruments sensitivity (Figs. 3 and 7). One can also notice that the C<sub>2</sub>H<sub>2</sub> and HCN peaks are higher in 2010. As South American biomass burning plumes are known to impact trace gases abundance above Reunion Island (Edwards et al., 2006a, b; Duflot et al., 2010), these 2010 higher peaks are probably due to the 2010 great Amazonian fires (Lewis et al., 2011) influence.

At Wollongong HCN peaks also in October–November due to the Southern Hemisphere biomass burning season (Paton-Walsh et al., 2010). We find maxima of around  $11 \times 10^{15} \text{ molec cm}^{-2}$  in October 2010, which is, similarly to Reunion Island, very likely to be a signature of the great Amazonian fires as South American biomass burning plumes are known to impact trace gases abundance above Australia (Edwards et al., 2006a, b). The seasonality and interannual variability matches well that of the ground-based FTIR measurements (correlation coefficient of 0.55 for the entire daily mean dataset, and of 0.83 for the monthly mean data set), with the IASI columns being biased low by  $0.48 \times 10^{15} \text{ molec cm}^{-2}$  (10%).

At Izaña HCN peaks in May–July due to the biomass burning activity occurring in Northern America and Europe (Sancho et al., 1992). We find maxima of around  $8 \times 10^{15} \text{ molec cm}^{-2}$ . The seasonality and interannual variability matches poorly that of the ground-based FTIR measurements for HCN (correlation coefficient of 0.28 for the entire daily mean dataset, and of 0.64 for the monthly mean data set), with the IASI columns being biased high by  $0.45 \times 10^{15} \text{ molec cm}^{-2}$  (11%). One can notice that HCN total columns as measured by ground-based FTIR are below the HCN stability threshold in boreal winter, which may result in erroneous IASI measurements (because unstable) and explain this poor match between the two datasets.

For C<sub>2</sub>H<sub>2</sub> at the Jungfraujoch site, the agreement between IASI and the ground-based retrieved columns is good (correlation coefficient of 0.70 for the entire daily mean



## Global measurements of HCN and C<sub>2</sub>H<sub>2</sub> from IASI

V. Dufлот et al.

Title Page

Abstract

Introduction

Conclusions

References

Tables

Figures



Back

Close

Full Screen / Esc

Printer-friendly Version

Interactive Discussion



- the transport pathway from Southern Africa to Australia in June-July-August (JJA) and September-October-November (SON) (Annegarn et al., 2002; Edwards et al., 2006a, b);
- the transport pathway linking South America (especially Amazonia) to Southern Africa and Australia during the SON period (Edwards et al., 2006a, b; Glatthor et al., 2015);
- the transport of the northern African plume over southern Asia to as far as the eastern Pacific by the northern subtropical jet during the MAM period (Glatthor et al., 2015);
- the Asian monsoon anticyclone (AMA), which is the dominant circulation feature in the Indian-Asian upper troposphere-lower stratosphere (UTLS) region during the Asian summer monsoon, spanning South East Asia to the Middle East and flanked by the equatorial and sub-tropical jets (Hoskins and Rodwell, 1995). The AMA is a known region of persistent enhanced pollution in the upper troposphere, linked to rapid vertical transport of surface air from Asia, India, and Indonesia in deep convection, and confinement by the strong anticyclonic circulation (Randel et al., 2010). The enhanced abundance of C<sub>2</sub>H<sub>2</sub> and HCN within the AMA in JJA observed by IASI is in accordance with previous studies (Park et al., 2008; Randel et al., 2010; Parker et al., 2011; Glatthor et al., 2015); however, one should keep in mind that this enhanced abundance measured by IASI is likely due to the combination of this pollution uplift and confinement with the higher sensitivity of the method in the upper troposphere (Fig. 2).

One can also notice the very good agreement between the seasonal HCN distributions shown in our Fig. 10 and the ones published recently in Glatthor et al. (2015, Fig. 3).

Figures 11 and 12 show the C<sub>2</sub>H<sub>2</sub> and HCN total columns time series, respectively, as measured by IASI (red dots) with the associated SD (light red lines) for each of the zones defined in Fig. 6.



## Global measurements of HCN and C<sub>2</sub>H<sub>2</sub> from IASI

V. Dufлот et al.

Title Page

Abstract

Introduction

Conclusions

References

Tables

Figures



Back

Close

Full Screen / Esc

Printer-friendly Version

Interactive Discussion



In Northern America, Europe and Boreal Central Asia (Fig. 11 – Zones NAM, EUR and BCA), C<sub>2</sub>H<sub>2</sub> peaks in late boreal winter due to the increased C<sub>2</sub>H<sub>2</sub> lifetime as already noticed over Jungfrauoch (Fig. 8). The boreal summer 2008 California wildfires event (Gyawali et al., 2009) is clearly visible in the NAM plot, as well as the August 2009 Russian wildfires in the NAM, EUR and BCA plots (Parrington et al., 2012; R'honi et al., 2013).

In North Central America (Fig. 12 – Zone NCA), the annual HCN peak in April–June is driven by local fire activity (van der Werf et al., 2010).

In South America, Southern Africa and Australia (Figs. 11 and 12 – Zones SAM, SAF and AUS), the Southern Hemisphere biomass burning season clearly drives the C<sub>2</sub>H<sub>2</sub> and HCN peaks in September–November each year. The signature of the great 2010 Amazonian fires (Lewis et al., 2011) is visible on each of the these three Zones, South American fire plumes being known to impact Southern Africa and Australia (Edwards et al., 2003, 2006a, b). The February 2009 Australian bush fires (Glatthor et al., 2013) are also noticeable on Zone AUS for both species.

In Northern Africa (Figs. 11 and 12 – Zone NAF), C<sub>2</sub>H<sub>2</sub> and HCN peak in boreal winter because of the biomass burning activity occurring in the Zone, and peak also in boreal summer because of the European and South Mediterranean fires (Van der Werf et al., 2010).

In South East Asia (Figs. 11 and 12 – Zone SEA), the observed C<sub>2</sub>H<sub>2</sub> and HCN peaks in July–September and January–March are due to local fire activity (Fortems-Cheiney et al., 2011; Magi et al., 2012). Additionally, the July–September peaks are also likely due to the combination of the pollution uplift and confinement within the AMA with the higher sensitivity of the method in the upper troposphere.

In Equatorial Asia (Figs. 11 and 12 – Zone EQA), local fire activity is visible in July–October, as well as the South East Asian fire activity in January–March (Fortems-Cheiney et al., 2011; Magi et al., 2012). The high biomass burning activity occurring in Indonesia from July to December 2009 (Yulianti et al., 2013; Hyer et al., 2013) is also clearly noticeable.

## Global measurements of HCN and C<sub>2</sub>H<sub>2</sub> from IASI

V. Dufлот et al.

Title Page

Abstract

Introduction

Conclusions

References

Tables

Figures



Back

Close

Full Screen / Esc

Printer-friendly Version

Interactive Discussion



C<sub>2</sub>H<sub>2</sub> and HCN sharing important common sources (cf. Introduction), the same annual and seasonal features are observed for both species. However, biomass burning being the major source for HCN (while it is biofuel and fossil fuel combustions for C<sub>2</sub>H<sub>2</sub>), one can notice the especially high increase in HCN abundance (up to  $13 \times 10^{15}$  molec cm<sup>-2</sup>) in the Southern Hemisphere during the austral biomass burning season (September to November). These observations are in accordance with previous studies (Lupu et al., 2009; Glatthor et al., 2009; Wiegele et al., 2012).

### 3.3 Comparison with model

In order to further evaluate the HCN and C<sub>2</sub>H<sub>2</sub> distributions retrieved from IASI spectra, they are compared in this section to the output of MOZART-4 for the years 2008–2010. We first describe the simulation set up before comparing simulated and observed distributions.

#### 3.3.1 MOZART-4 simulation set up

The model simulations presented here are performed with the MOZART-4 global 3-D chemical transport model (Emmons et al., 2010a), which is driven by assimilated meteorological fields from the NASA Global Modeling and Assimilation Office (GMAO) Goddard Earth Observing System (GEOS). MOZART-4 was run with a horizontal resolution of 1.875° latitude × 2.5° longitude, with 56 levels in the vertical and with its standard chemical mechanism (see Emmons et al., 2010a, for details). The model simulations have been initialized by simulations starting in July 2007 to avoid contamination by the spin-up in the model results. MOZART-4 simulations of numerous species (CO, O<sub>3</sub> and related tracers including C<sub>2</sub>H<sub>2</sub>) have been previously compared to in situ and satellite observations and used to track the intercontinental transport of pollution (e.g., Emmons et al., 2010b; Pfister et al., 2006, 2008, 2011; Tilmes et al., 2011; Clarisse et al., 2011b; Wespes et al., 2012).



information, we rather applied on each of the MOZART-4 simulated profiles the Jacobians of the used forward model (cf. Sect. 2.2.3 and Fig. 3) to take into account the sensitivity of both the radiative transfer model and IASI. Note that here again HCN abundances below  $2.8 \times 10^{15}$  molec $\text{cm}^{-2}$  have been removed from both space measurements and simulated columns to allow comparison of both datasets (cf. Sect. 2.2.3).

MOZART-4 simulations can be evaluated by looking at Figs. 9 and 11 for  $\text{C}_2\text{H}_2$ , and Figs. 10 and 12 for HCN. Figures 11 and 12 show the simulated  $\text{C}_2\text{H}_2$  and HCN total columns time series, respectively, for each of the zones defined in Fig. 6 superimposed to IASI observations. Table 2 summarizes the biases and correlation coefficients resulting from the comparison between model and observations. Looking at these Table and Figures, the following conclusions can be drawn:

- seasonal cycles observed from satellite data are reasonably well reproduced by the model;
- the African, South American, Asian and Indonesian hot spots are clearly visible in the model;
- exceptional events that are captured by IASI (cf. Sect. 3.2) are not simulated by MOZART-4;
- the model is more negatively biased in the Southern Hemisphere (Bias =  $-61\%$  for  $\text{C}_2\text{H}_2$  and Bias =  $-25\%$  for HCN) than in the Northern Hemisphere (Bias =  $40\%$  for  $\text{C}_2\text{H}_2$  and Bias =  $-3\%$  for HCN), suggesting that anthropogenic (biomass burning) emissions are likely overestimated (underestimated) in the model;
- the model reasonably reproduces the main transport pathways identified on IASI observations (cf. Sect. 3.2). However, the low background concentrations in the Southern Hemisphere as simulated by the model, especially for Southern Africa and Australia (Figs. 11 and 12 – Zones SAF and AUS), suggest that the model transportation scheme and/or the modeled species' lifetime still can be improved to simulate the impact of their long range transport.

Global measurements of HCN and  $\text{C}_2\text{H}_2$  from IASI

V. Dufлот et al.

Title Page

Abstract

Introduction

Conclusions

References

Tables

Figures



Back

Close

Full Screen / Esc

Printer-friendly Version

Interactive Discussion



In Table 2, for  $C_2H_2$ , the correlation coefficients are good ( $\geq 0.6$ ) to very good ( $\geq 0.9$ ) except for the zones SAM (South America), SEA (South East Asia) and EQA (Equatorial Asia). For HCN, the correlation coefficients are good ( $\geq 0.6$ ) except for the zones NCA (North Central America), NAF (Northern Africa), SEA and EQA.

For South America (Zone SAM), correlation coefficient is not as good for  $C_2H_2$  ( $R = 0.54$ ) due to a backward shift of the species abundance peaks in years 2008 and 2009: in the model, this increase occurs from July to October while observations (and previous studies, e.g. van der Werf et al., 2010) show an increase from August to December. This backward shift is also visible for HCN (Fig. 12), but to a lesser extent.

For South East Asia and Equatorial Asia (Zones SEA and EQA), the low correlation coefficients (cf. Table 2) can be attributed to the difficulty of locating precisely with the model the intercontinental convergence zone (ITCZ) which drives the long-range transport of  $C_2H_2$  and HCN-loaded plumes into the zone. Additionally, for Equatorial Asia, the too low fire emissions considered in the model for Indonesia from July to December 2009 may also be a cause for these low correlation coefficients.

For HCN in northern Africa (Zone NAF), correlation coefficient is very low ( $R = 0.07$ ) because the model sets the abundance peaks around August while observations show peaks occurring around December, which is in accordance with previous studies (van der Werf et al., 2010). This inadequate timing for HCN in the model simulations could be due to an overestimation of the Southern African contribution to the Northern African loading and is visible on Fig. 10 (JJA).

## 4 Conclusions

We have presented a fast method to retrieve HCN and  $C_2H_2$  total columns from IASI spectra. The sensitivity of this method to the two species is mostly in the mid-upper troposphere. With this method,  $C_2H_2$  total columns can be retrieved globally with 5% precision, while HCN abundances can be retrieved for abundances greater than

Global  
measurements of  
HCN and  $C_2H_2$  from  
IASI

V. Dufлот et al.

Title Page

Abstract

Introduction

Conclusions

References

Tables

Figures

◀

▶

◀

▶

Back

Close

Full Screen / Esc

Printer-friendly Version

Interactive Discussion



$0.28 \times 10^{16} \text{ molec cm}^{-2}$  with 10 % precision in the  $\pm 20^\circ$  latitudinal band and with 30 % precision in the  $[\pm 35^\circ : \pm 20^\circ]$  latitudinal band.

Total columns have been retrieved globally for a three year period and compared to routine FTIR measurements available at Reunion Island (HCN and  $\text{C}_2\text{H}_2$ ), Wollongong (HCN), Jungfraujoch ( $\text{C}_2\text{H}_2$ ), and Izaña (HCN). The comparison between IASI and FTIR retrieved total columns demonstrates the capabilities of IASI to capture the seasonality in HCN and  $\text{C}_2\text{H}_2$  in most cases.

Global seasonal distributions, as well as regional time series of the total columns, have been shown for the two species. IASI is able to capture persisting, seasonal and exceptional features for both species, and the observed patterns are in a general good agreement with previous spaceborne studies (ACE-FTS and MIPAS).

The comparison between these observations and MOZART-4 simulations leads to the following conclusions: (i) the model is able to capture most of the hot spots and seasonal cycles, but not the exceptional events, (ii) the model seems to overestimate (underestimate) anthropogenic (biomass burning) emissions for both species, (iii) the model dynamical scheme and/or the modeled species lifetime could be improved to simulate the impact of the long range transport for these species.

*Acknowledgements.* IASI has been developed and built under the responsibility of the Centre National d'Etudes Spatiales (CNES, France). It is flown onboard the MetOp satellites as part of the EUMETSAT Polar System. The IASI L1 data are received through the EUMETSAT-Cast near real time data distribution service. Part of the research is supported by EUMETSAT through the O3SAF project. P. F. C. is Senior Research Associate and L.C. is Research Associate at the F.R.S.-FNRS. The research in Belgium was funded by the F.R.S.-FNRS, the Belgian Science Policy Office, and the European Space Agency (ESA Prodex arrangements and the AGACC-II project). The Australian Research Council has provided financial support over the years for the NDACC site at Wollongong, most recently as part of project DP110101948. The Liège team further acknowledges the Fédération Wallonie-Bruxelles for supporting travel costs to the Jungfraujoch station and wishes to thank the International Foundation High Altitude Research Stations Jungfraujoch and Gornergrat (HFSJG, Bern) for supporting the facilities needed to perform the observations. Since 1999, the Izaña FTIR activities have been

Global measurements of HCN and  $\text{C}_2\text{H}_2$  from IASI

V. Dufлот et al.

Title Page

Abstract

Introduction

Conclusions

References

Tables

Figures



Back

Close

Full Screen / Esc

Printer-friendly Version

Interactive Discussion



supported by different funding agencies: European Commission, European Research Council, European Space Agency, EUMETSAT, Deutsche Forschungsgemeinschaft, Deutsches Zentrum für Luft- und Raumfahrt, and the Ministerios de Ciencia e Innovación and Educación from Spain. The authors also wish to thank the French regional, national (INSU, CNRS), and international (NASA/GFSC) organizations for supporting the OPAR (Observatoire de Physique de l'Atmosphère de la Réunion) station. The NDACC is also acknowledged for providing consistent and well documented datasets.

## References

- Anderson, G. P., Clough, S. A., Kneizys, F. X., Chetwynd, J. H., and Shettle, E. P.: AFGL Atmospheric Constituent Profiles (0–120 km), Environmental Research Papers no. 954, Air Force Geophysics Laboratory, Hanscom AFB Massachusetts, AFGL TR-86-0110, 1986.
- Annegarn, H. J., Otter L., Swap R. J., and Scholes R. J.: Southern Africa's ecosystem in a test-tube – a perspective on the Southern African Regional Science Initiative (SAFARI 2000), *S. Afr. J. Sci.*, 98, 111–113, 2002.
- Cicerone, R. J. and Zellner, R.: The atmospheric chemistry of hydrogen cyanide (HCN), *J. Geophys. Res.*, 88, 10689–10696, 1983.
- Clarisse, L., Coheur, P. F., Prata, A. J., Hurtmans, D., Razavi, A., Phulpin, T., Hadji-Lazaro, J., and Clerbaux, C.: Tracking and quantifying volcanic SO<sub>2</sub> with IASI, the September 2007 eruption at Jebel at Tair, *Atmos. Chem. Phys.*, 8, 7723–7734, doi:10.5194/acp-8-7723-2008, 2008.
- Clarisse, L., Clerbaux, C., Dentener, F., Hurtmans, D., and Coheur, P.-F.: Global ammonia distribution derived from infrared satellite observations, *Nat. Geosci.*, 2, 479–483, doi:10.1038/NGEO551, 2009.
- Clarisse, L., R'honi, Y., Coheur, P.-F., Hurtmans, D., and Clerbaux, C.: Thermal infrared nadir observations of 24 atmospheric gases, *Geophys. Res. Lett.*, 38, L10802, doi:10.1029/2011GL047271, 2011a.
- Clarisse, L., Formm, M., Ngadi, Y., Emmons, L., Clerbaux, C., Hurtmans, D., and Coheur, P. F.: Intercontinental transport of anthropogenic sulfur dioxide and other pollutants: an infrared remote sensing case study, *Geophys. Res. Lett.* 38, L19806, doi:10.1029/2011GL048976, 2011b.

**Global  
measurements of  
HCN and C<sub>2</sub>H<sub>2</sub> from  
IASI**

V. Dufлот et al.

Title Page

Abstract

Introduction

Conclusions

References

Tables

Figures



Back

Close

Full Screen / Esc

Printer-friendly Version

Interactive Discussion



Clerbaux, C., Boynard, A., Clarisse, L., George, M., Hadji-Lazaro, J., Herbin, H., Hurtmans, D., Pommier, M., Razavi, A., Turquety, S., Wespes, C., and Coheur, P.-F.: Monitoring of atmospheric composition using the thermal infrared IASI/MetOp sounder, *Atmos. Chem. Phys.*, 9, 6041–6054, doi:10.5194/acp-9-6041-2009, 2009.

5 Coheur, P.-F., Barret, B., Turquety, S., Hurtmans, D., Hadji-Lazaro, J., and Clerbaux, C.: Retrieval and characterization of ozone vertical profiles from a thermal infrared nadir sounder, *J. Geophys. Res.*, 110, D24303, doi:10.1029/2005JD005845, 2005.

Dufлот, V., Dils, B., Baray, J. L., De Mazière, M., Attié, J. L., Vanhaelewyn, G., Senten, C., Vigouroux, C., Clain, G., and Delmas, R.: Analysis of the origin of the distribution of CO in the subtropical southern Indian Ocean in 2007, *J. Geophys. Res.*, 115, D22106, doi:10.1029/2010JD013994, 2010.

Dufлот, V., Hurtmans, D., Clarisse, L., R'honi, Y., Vigouroux, C., De Mazière, M., Mahieu, E., Servais, C., Clerbaux, C., and Coheur, P.-F.: Measurements of hydrogen cyanide (HCN) and acetylene (C<sub>2</sub>H<sub>2</sub>) from the Infrared Atmospheric Sounding Interferometer (IASI), *Atmos. Meas. Tech.*, 6, 917–925, doi:10.5194/amt-6-917-2013, 2013.

15 Edwards, D. P., Lamarque, J.-F., Attié, J.-L., Emmons, L. K., Richter, A., Cammas, J.-P., Gille, J. C., Francis, G. L., Deeter, M. N., Warner, J., Ziskin, D. C., Lyjak, L. V., Drummond, J. R., and Burrows, J. P.: Tropospheric ozone over the tropical Atlantic: a satellite perspective, *J. Geophys. Res.*, 108, 4237, doi:10.1029/2002JD002927, 2003.

20 Edwards, D. P., Emmons, L. K., Gille, J. C., Chu, A., Attié, J.-L., Giglio, L., Wood, S. W., Haywood, J., Deeter, M. N., Massie, S. T., Ziskin, D. C., and Drummond, J. R.: Satellite-observed pollution from Southern Hemisphere biomass burning, *J. Geophys. Res.*, 111, D14312, doi:10.1029/2005JD006655, 2006a.

25 Edwards, D. P., Emmons, L. K., Gille, J. C., Chu, A., Attié, J.-L., Giglio, L., Wood, S. W., Haywood, J., Deeter, M. N., Massie, S. T., Ziskin, D. C., and Drummond, J. R.: Satellite-observed pollution from Southern Hemisphere biomass burning, *J. Geophys. Res.*, 111, D14312, doi:10.1029/2005JD006655, 2006b.

30 Emmons, L. K., Walters, S., Hess, P. G., Lamarque, J.-F., Pfister, G. G., Fillmore, D., Granier, C., Guenther, A., Kinnison, D., Laepple, T., Orlando, J., Tie, X., Tyndall, G., Wiedinmyer, C., Baughcum, S. L., and Kloster, S.: Description and evaluation of the Model for Ozone and Related chemical Tracers, version 4 (MOZART-4), *Geosci. Model Dev.*, 3, 43–67, doi:10.5194/gmd-3-43-2010, 2010a.



**Global  
measurements of  
HCN and C<sub>2</sub>H<sub>2</sub> from  
IASI**

V. Dufлот et al.

Title Page

Abstract

Introduction

Conclusions

References

Tables

Figures



Back

Close

Full Screen / Esc

Printer-friendly Version

Interactive Discussion

Emmons, L. K., Apel, E. C., Lamarque, J.-F., Hess, P. G., Avery, M., Blake, D., Brune, W., Campos, T., Crawford, J., DeCarlo, P. F., Hall, S., Heikes, B., Holloway, J., Jimenez, J. L., Knapp, D. J., Kok, G., Mena-Carrasco, M., Olson, J., O'Sullivan, D., Sachse, G., Walega, J., Weibring, P., Weinheimer, A., and Wiedinmyer, C.: Impact of Mexico City emissions on regional air quality from MOZART-4 simulations, *Atmos. Chem. Phys.*, 10, 6195–6212, doi:10.5194/acp-10-6195-2010, 2010b.

Fortems-Cheiney, A., Chevallier, F., Pison, I., Bousquet, P., Szopa, S., Deeter, M. N., and Clerbaux, C.: Ten years of CO emissions as seen from Measurements of Pollution in the Troposphere (MOPITT), *J. Geophys. Res.*, 116, D05304, doi:10.1029/2010JD014416, 2011.

Glatthor, N., von Clarmann, T., Stiller, G. P., Funke, B., Koukouli, M. E., Fischer, H., Grabowski, U., Höpfner, M., Kellmann, S., and Linden, A.: Large-scale upper tropospheric pollution observed by MIPAS HCN and C<sub>2</sub>H<sub>6</sub> global distributions, *Atmos. Chem. Phys.*, 9, 9619–9634, doi:10.5194/acp-9-9619-2009, 2009.

Glatthor, N., Höpfner, M., Semeniuk, K., Lupu, A., Palmer, P. I., McConnell, J. C., Kaminski, J. W., von Clarmann, T., Stiller, G. P., Funke, B., Kellmann, S., Linden, A., and Wiegele, A.: The Australian bushfires of February 2009: MIPAS observations and GEM-AQ model results, *Atmos. Chem. Phys.*, 13, 1637–1658, doi:10.5194/acp-13-1637-2013, 2013.

Glatthor, N., Höpfner, M., Stiller, G. P., von Clarmann, T., Funke, B., Lossow, S., Eckert, E., Grabowski, U., Kellmann, S., Linden, A., A. Walker, K., and Wiegele, A.: Seasonal and inter-annual variations in HCN amounts in the upper troposphere and lower stratosphere observed by MIPAS, *Atmos. Chem. Phys.*, 15, 563–582, doi:10.5194/acp-15-563-2015, 2015.

González Abad, G., Allen, N. D. C., Bernath, P. F., Boone, C. D., McLeod, S. D., Manney, G. L., Toon, G. C., Carouge, C., Wang, Y., Wu, S., Barkley, M. P., Palmer, P. I., Xiao, Y., and Fu, T. M.: Ethane, ethyne and carbon monoxide concentrations in the upper troposphere and lower stratosphere from ACE and GEOS-Chem: a comparison study, *Atmos. Chem. Phys.*, 11, 9927–9941, doi:10.5194/acp-11-9927-2011, 2011.

Guenther, A., Karl, T., Harley, P., Wiedinmyer, C., Palmer, P. I., and Geron, C.: Estimates of global terrestrial isoprene emissions using MEGAN (Model of Emissions of Gases and Aerosols from Nature), *Atmos. Chem. Phys.*, 6, 3181–3210, doi:10.5194/acp-6-3181-2006, 2006.

Gyawali, M., Arnott, W. P., Lewis, K., and Moosmüller, H.: In situ aerosol optics in Reno, NV, USA during and after the summer 2008 California wildfires and the influence of absorbing

**Global  
measurements of  
HCN and C<sub>2</sub>H<sub>2</sub> from  
IASI**

V. Dufлот et al.

Title Page

Abstract

Introduction

Conclusions

References

Tables

Figures



Back

Close

Full Screen / Esc

Printer-friendly Version

Interactive Discussion

and non-absorbing organic coatings on spectral light absorption, *Atmos. Chem. Phys.*, 9, 8007–8015, doi:10.5194/acp-9-8007-2009, 2009.

Hoskins, B. J. and Rodwell, M. J.: A model of the Asian summer monsoon, part I: the global scale, *J. Atmos. Sci.*, 52, 1329–1340, 1995.

5 Hyer, E. J., Reid, J. S., Prins, E. M., Hoffman, J. P., Schmidt, C. C., Miettinen, J. I., and Giglio, L.: Patterns of fire activity over Indonesia and Malaysia from polar and geostationary satellite observations, *Atmos. Res.*, 122, 504–519, 2013.

Lamarque, J.-F., Hess, P., Emmons, L., Buja, L., Washington, W., and Granier, C.: Tropospheric ozone evolution between 1890 and 1990, *J. Geophys. Res.*, 110, D08304, doi:10.1029/2004JD005537, 2005.

10 Lewis, S. L., Brando, P. M., Phillips, O. L., van der Heijden, G. M. F., and Nepstad, D.: The 2010 Amazon drought, *Science*, 331, 554, doi:10.1126/science.1200807, 2011.

Li, Q., Jacob, D., Bey, I., Yantosca, R., Zhao, Y., Kondo, Y., and Notholt, J.: Atmospheric hydrogen cyanide (HCN): biomass burning source, ocean sink?, *Geophys. Res. Lett.*, 27, 357–360, 2000.

15 Li, Q., Palmer, P. I., Pumphrey, H. C., Bernath, P., and Mahieu, E.: What drives the observed variability of HCN in the troposphere and lower stratosphere?, *Atmos. Chem. Phys.*, 9, 8531–8543, doi:10.5194/acp-9-8531-2009, 2009.

Logan, J. A., Prather, M. J., Wofsy, S. C., and McElroy, M. B.: Tropospheric chemistry: a global perspective, *J. Geophys. Res.*, 86, 7210–7254, 1981.

20 Lupu, A., Kaminski, J. W., Neary, L., McConnell, J. C., Toyota, K., Rinsland, C. P., Bernath, P. F., Walker, K. A., Boone, C. D., Nagahama, Y., and Suzuki, K.: Hydrogen cyanide in the upper troposphere: GEM-AQ simulation and comparison with ACE-FTS observations, *Atmos. Chem. Phys.*, 9, 4301–4313, doi:10.5194/acp-9-4301-2009, 2009.

25 Magi, B. I., Rabin, S., Shevliakova, E., and Pacala, S.: Separating agricultural and non-agricultural fire seasonality at regional scales, *Biogeosciences*, 9, 3003–3012, doi:10.5194/bg-9-3003-2012, 2012.

Mahieu, E., Duchatelet, P., Bernath, P. F., Boone, C. D., De Mazière, M., Demoulin, P., Rinsland, C. P., Servais, C., and Walker, K. A.: Retrievals of C<sub>2</sub>H<sub>2</sub> from high-resolution FTIR solar spectra recorded at the Jungfraujoch station (46.5° N) and comparison with ACE-FTS observations, *Geophys. Res. Abstr.*, 10, available at: <http://hdl.handle.net/2268/15191> (last access: 21 May 2015), 2008.

---

**Global  
measurements of  
HCN and C<sub>2</sub>H<sub>2</sub> from  
IASI**V. Dufлот et al.

---

[Title Page](#)[Abstract](#)[Introduction](#)[Conclusions](#)[References](#)[Tables](#)[Figures](#)[⏪](#)[⏩](#)[◀](#)[▶](#)[Back](#)[Close](#)[Full Screen / Esc](#)[Printer-friendly Version](#)[Interactive Discussion](#)

Mei, L., Xue, Y., de Leeuw, G., Guang, J., Wang, Y., Li, Y., Xu, H., Yang, L., Hou, T., He, X., Wu, C., Dong, J., and Chen, Z.: Integration of remote sensing data and surface observations to estimate the impact of the Russian wildfires over Europe and Asia during August 2010, *Biogeosciences*, 8, 3771–3791, doi:10.5194/bg-8-3771-2011, 2011.

5 Park, M., Randel, W. J., Emmons, L. K., Bernath, P. F., Walker, K. A., and Boone, C. D.: Chemical isolation in the Asian monsoon anticyclone observed in Atmospheric Chemistry Experiment (ACE-FTS) data, *Atmos. Chem. Phys.*, 8, 757–764, doi:10.5194/acp-8-757-2008, 2008.

Parker, R. J., Remedios, J. J., Moore, D. P., and Kanawade, V. P.: Acetylene C<sub>2</sub>H<sub>2</sub> retrievals from MIPAS data and regions of enhanced upper tropospheric concentrations in August 2003, *Atmos. Chem. Phys.*, 11, 10243–10257, doi:10.5194/acp-11-10243-2011, 2011.

10 Parrington, M., Palmer, P. I., Henze, D. K., Tarasick, D. W., Hyer, E. J., Owen, R. C., Helmig, D., Clerbaux, C., Bowman, K. W., Deeter, M. N., Barratt, E. M., Coheur, P.-F., Hurtmans, D., Jiang, Z., George, M., and Worden, J. R.: The influence of boreal biomass burning emissions on the distribution of tropospheric ozone over North America and the North Atlantic during 2010, *Atmos. Chem. Phys.*, 12, 2077–2098, doi:10.5194/acp-12-2077-2012, 2012.

Paton-Walsh, C., Deutscher, N. M., Griffith, D. W. T., Forgan, B. W., Wilson, S. R., Jones, N. B., and Edwards, D. P.: Trace gas emissions from savanna fires in northern Australia, *J. Geophys. Res.*, 115, D16314, doi:10.1029/2009JD013309, 2010.

20 Pfister, G. G., Emmons, L. K., Hess, P. G., Honrath, R., Lamarque, J.-F., Val Martin, M., Owen, R. C., Avery, M. A., Browell, E. V., Holloway, J. S., Nédélec, P., Purvis, R., Ryrson, T. B., Sachse, G. W., and Schlager, H.: Ozone production from the 2004 North American boreal fires, *J. Geophys. Res.*, 111, D24S07, doi:10.1029/2006JD007695, 2006.

Pfister, G. G., Emmons, L. K., Hess, P. G., Lamarque, J.-F., Thompson, A. M., and Yorks, J. E.: Analysis of the summer 2004 ozone budget over the United States using Intercontinental Transport Experiment Ozone-sonde Network Study (IONS) observations and Model of Ozone and Related Tracers (MOZART-4) simulations, *J. Geophys. Res.*, 113, D23306, doi:10.1029/2008JD010190, 2008.

25 Pfister, G. G., Parrish, D. D., Worden, H., Emmons, L. K., Edwards, D. P., Wiedinmyer, C., Diskin, G. S., Huey, G., Oltmans, S. J., Thouret, V., Weinheimer, A., and Wisthaler, A.: Characterizing summertime chemical boundary conditions for air masses entering the US West Coast, *Atmos. Chem. Phys.*, 11, 1769–1790, doi:10.5194/acp-11-1769-2011, 2011.

## Global measurements of HCN and C<sub>2</sub>H<sub>2</sub> from IASI

V. Dufлот et al.

Title Page

Abstract

Introduction

Conclusions

References

Tables

Figures



Back

Close

Full Screen / Esc

Printer-friendly Version

Interactive Discussion



- Pumphrey, H. C., Santee, M. L., Livesey, N. J., Schwartz, M. J., and Read, W. G.: Microwave Limb Sounder observations of biomassburning products from the Australian bush fires of February 2009, *Atmos. Chem. Phys.*, 11, 6285–6296, doi:10.5194/acp-11-6285-2011, 2011.
- Randel, W. J., Park, M., Emmons, L., Kinnison, D., Bernath, P., Walker, K. A., Boone, C., and Pumphrey, H.: Asian monsoon transport of pollution to the stratosphere, *Science*, 328, 611–613, doi:10.1126/science.1182274, 2010.
- R'Honi, Y., Clarisse, L., Clerbaux, C., Hurtmans, D., Dufлот, V., Turquety, S., Ngadi, Y., and Coheur, P.-F.: Exceptional emissions of NH<sub>3</sub> and HCOOH in the 2010 Russian wildfires, *Atmos. Chem. Phys.*, 13, 4171–4181, doi:10.5194/acp-13-4171-2013, 2013.
- Rodgers, C. D.: *Inverse Methods for Atmospheric Sounding: Theory and Practice*, Series on Atmospheric, Oceanic and Planetary Physics – Vol. 2, World Scientific Publishing CO, Singapore, 2000.
- Sancho, P., De La Cruz, J., Diaz, A., Martin, F., Hernandez, E., Valero, F., and Albarran, B.: A five-year climatology of back-trajectories from the Izaña baseline station, Tenerife, Canary Islands, *Atmos. Environ.*, 26A, 1081–1096, 1992.
- Sauvage, B., Thouret, V., Cammas, J.-P., Gheusi, F., Athier, G., and Nédélec, P.: Tropospheric ozone over Equatorial Africa: regional aspects from the MOZAIC data, *Atmos. Chem. Phys.*, 5, 311–335, doi:10.5194/acp-5-311-2005, 2005.
- Singh, H. B., Salas, L., Herlth, D., Kolyer, R., Czech, E., Vizee, W., Li, Q., Jacob, D. J., Blake, D., Sachse, G., Harward, C. N., Fuelberg, H., Kiley, C. M., Zhao, Y., and Kondo, Y.: In situ measurements of HCN and CH<sub>3</sub>CN over the Pacific Ocean: sources, sinks and budgets, *J. Geophys. Res.*, 108, 8795, doi:10.1029/2002JD003006, 2003.
- Standard Atmosphere 1976, National Oceanic and Atmospheric Administration, National Aeronautics and Space Administration, U.S. Air Force, U.S. Government Printing Office, NOAA-S/T 76-1562, Washington, DC, 228 pp., 1976.
- Tilmes, S., Emmons, L. K., Law, K. S., Ancellet, G., Schlager, H., Paris, J.-D., Fuelberg, H. E., Streets, D. G., Wiedinmyer, C., Diskin, G. S., Kondo, Y., Holloway, J., Schwarz, J. P., Spackman, J. R., Campos, T., Nédélec, P., and Panchenko, M. V.: Source contributions to Northern Hemisphere CO and black carbon during spring and summer 2008 from POLARCAT and START08/preHIPPO observations and MOZART-4, *Atmos. Chem. Phys. Discuss.*, 11, 5935–5983, doi:10.5194/acpd-11-5935-2011, 2011.
- Van Damme, M., Clarisse, L., Heald, C. L., Hurtmans, D., Ngadi, Y., Clerbaux, C., Dolman, A. J., Erisman, J. W., and Coheur, P. F.: Global distributions, time series and error characterization

**Global  
measurements of  
HCN and C<sub>2</sub>H<sub>2</sub> from  
IASI**

V. Dufлот et al.

Title Page

Abstract

Introduction

Conclusions

References

Tables

Figures



Back

Close

Full Screen / Esc

Printer-friendly Version

Interactive Discussion

of atmospheric ammonia (NH<sub>3</sub>) from IASI satellite observations, *Atmos. Chem. Phys.*, 14, 2905–2922, doi:10.5194/acp-14-2905-2014, 2014.

van der Werf, G. R., Randerson, J. T., Giglio, L., Collatz, G. J., Kasibhatla, P. S., and Arellano Jr., A. F.: Interannual variability in global biomass burning emission from 1997 to 2004, *Atmos. Chem. Phys.*, 6, 3423–3441, doi:10.5194/acp-6-3423-2006, 2006.

van der Werf, G. R., Randerson, J. T., Giglio, L., Collatz, G. J., Mu, M., Kasibhatla, P. S., Morton, D. C., DeFries, R. S., Jin, Y., and van Leeuwen, T. T.: Global fire emissions and the contribution of deforestation, savanna, forest, agricultural, and peat fires (1997–2009), *Atmos. Chem. Phys.*, 10, 11707–11735, doi:10.5194/acp-10-11707-2010, 2010.

Vigouroux, C., Stavrakou, T., Whaley, C., Dils, B., Dufлот, V., Hermans, C., Kumps, N., Metzger, J.-M., Scolas, F., Vanhaelewyn, G., Müller, J.-F., Jones, D. B. A., Li, Q., and De Mazière, M.: FTIR time-series of biomass burning products (HCN, C<sub>2</sub>H<sub>6</sub>, C<sub>2</sub>H<sub>2</sub>, CH<sub>3</sub>OH, and HCOOH) at Reunion Island (21° S, 55° E) and comparisons with model data, *Atmos. Chem. Phys.*, 12, 10367–10385, doi:10.5194/acp-12-10367-2012, 2012.

Volkamer, R., Ziemann, P. J., and Molina, M. J.: Secondary organic aerosol formation from acetylene (C<sub>2</sub>H<sub>2</sub>), seed effect on SOA yields due to organic photochemistry in the aerosol aqueous phase, *Atmos. Chem. Phys.*, 9, 1907–1928, doi:10.5194/acp-9-1907-2009, 2009.

Walker, J.C, Dudhia, A., and Carboni, E.: An effective method for the detection of trace species demonstrated using the MetOp Infrared Atmospheric Sounding Interferometer, *Atmos. Meas. Tech.*, 4, 1567–1580, doi:10.5194/amt-4-1567-2011, 2011.

Wespes, C., Emmons, L., Edwards, D. P., Hannigan, J., Hurtmans, D., Saunio, M., Coheur, P.-F., Clerbaux, C., Coffey, M. T., Batchelor, R. L., Lindenmaier, R., Strong, K., Weinheimer, A. J., Nowak, J. B., Ryerson, T. B., Crouse, J. D., and Wennberg, P. O.: Analysis of ozone and nitric acid in spring and summer Arctic pollution using aircraft, ground-based, satellite observations and MOZART-4 model: source attribution and partitioning, *Atmos. Chem. Phys.*, 12, 237–259, doi:10.5194/acp-12-237-2012, 2012.

Wiedinmyer, C., Quayle, B., Geron, C., Belote, A., McKenzie, D., Zhang, X., O'Neill, S., and Wynne, K.: Estimating emissions from fires in North America for air quality modeling, *Atmos. Environ.*, 40, 3419–3432, 2006.

Wiedinmyer, C., Akagi, S. K., Yokelson, R. J., Emmons, L. K., Al-Saadi, J. A., Orlando, J. J., and Soja, A. J.: The Fire INventory from NCAR (FINN): a high resolution global model to estimate the emissions from open burning, *Geosci. Model Dev.*, 4, 625–641, doi:10.5194/gmd-4-625-2011, 2011.

**Global  
measurements of  
HCN and C<sub>2</sub>H<sub>2</sub> from  
IASI**

V. Dufлот et al.

[Title Page](#)[Abstract](#)[Introduction](#)[Conclusions](#)[References](#)[Tables](#)[Figures](#)[Back](#)[Close](#)[Full Screen / Esc](#)[Printer-friendly Version](#)[Interactive Discussion](#)

- Wiegele, A., Glatthor, N., Höpfner, M., Grabowski, U., Kellmann, S., Linden, A., Stiller, G., and von Clarmann, T.: Global distributions of C<sub>2</sub>H<sub>6</sub>, C<sub>2</sub>H<sub>2</sub>, HCN, and PAN retrieved from MIPAS reduced spectral resolution measurements, *Atmos. Meas. Tech.*, 5, 723–734, doi:10.5194/amt-5-723-2012, 2012.
- 5 Xiao, Y., Jacob, D. J., and Turquety, S.: Atmospheric acetylene and its relationship with CO as an indicator of air mass age, *J. Geophys. Res.-Atmos.*, 112, D12305, doi:10.1029/2006JD008268, 2007.
- Yienger, J. J., M. Galanter, T. A. Holloway, M. J. Phadnis, S. K. Guttikunda, G. R. Carmichael, W. J. Moxim, and Levy II, H.: The episodic nature of air pollution transport from
- 10 Asia to North America, *J. Geophys. Res.*, 105, 2693126945, doi:10.1029/2000JD900309, 2000.
- Yulianti, N. and Hayasaka, H.: Recent active fires under El Niño conditions in Kalimantan, Indonesia, *Am. J. Plant Sci.*, 4, 685–696, 2013.
- Zander, R., Rinsland, C. P., Ehhalt, D. H., Rudolph, J., and Demoulin P. H.: Vertical column abundances and seasonal cycle of acetylene, C<sub>2</sub>H<sub>2</sub>, above the Jungfraujoch Station, derived from IR solar observations, *J. Atm. Chem.*, 13, 359–372, 1991.
- 15 Zhang, Q., Streets, D. G., Carmichael, G. R., He, K. B., Huo, H., Kannari, A., Klimont, Z., Park, I. S., Reddy, S., Fu, J. S., Chen, D., Duan, L., Lei, Y., Wang, L. T., and Yao, Z. L.: Asian emissions in 2006 for the NASA INTEX-B mission, *Atmos. Chem. Phys.*, 9, 5131–5153, doi:10.5194/acp-9-5131-2009, 2009.
- 20

## Global measurements of HCN and C<sub>2</sub>H<sub>2</sub> from IASI

V. Dufлот et al.

Title Page

Abstract

Introduction

Conclusions

References

Tables

Figures

◀

▶

◀

▶

Back

Close

Full Screen / Esc

Printer-friendly Version

Interactive Discussion



**Table 1.** Global C<sub>2</sub>H<sub>2</sub> and HCN emission sources (Tg(species) year<sup>-1</sup>) during the period 2008–2010 from the dataset used in MOZART-4.

Sources/Year	C <sub>2</sub> H <sub>2</sub>			HCN		
	2008	2009	2010	2008	2009	2010
Anthropogenic	3.37	3.37	3.37	1.67	1.67	1.67
Biomass Burning	0.64	0.71	0.83	1.38	1.33	1.58
Total	4.01	4.07	4.20	3.05	3.00	3.25

## Global measurements of HCN and C<sub>2</sub>H<sub>2</sub> from IASI

V. Dufлот et al.

**Table 2.** Correlation coefficients ( $R$ ) and biases (Bias) between IASI observations and MOZART-4 simulations for each of the zones defined in Fig. 6.

Zones	C <sub>2</sub> H <sub>2</sub>		HCN	
	$R$	Bias (%)	$R$	Bias (%)
NAM	0.93	47	–	–
NCA	–	–	0.44	–1
SAM	0.54	–50	0.76	–14
EUR	0.88	115	–	–
NAF	0.66	–35	0.07	–2
SAF	0.69	–67	0.86	–28
BCA	0.82	105	–	–
SEA	–0.31	–23	0.57	–4
EQA	0.45	–51	0.09	–27
AUS	0.65	–61	0.77	–26
Global	0.72	–1	0.69	–16

Title Page

Abstract

Introduction

Conclusions

References

Tables

Figures

◀

▶

◀

▶

Back

Close

Full Screen / Esc

Printer-friendly Version

Interactive Discussion





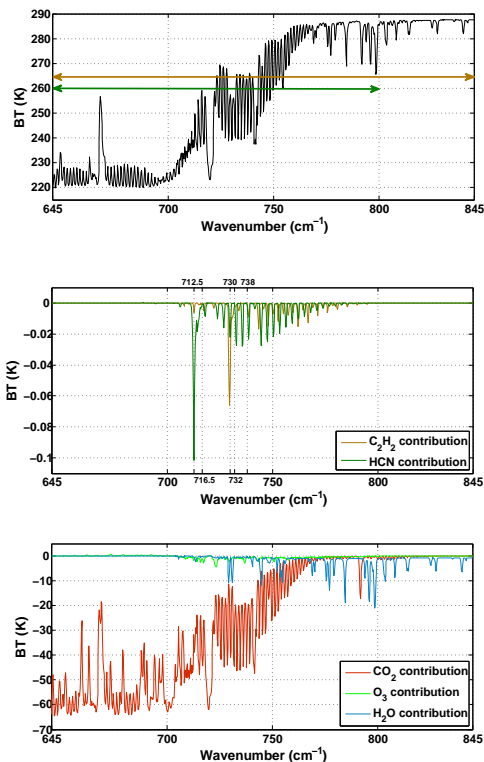


**Figure 1.** (Top) Simulated spectra in the region of the HCN  $\nu_2$  band and  $C_2H_2$   $\nu_5$  band. The green (brown) double sided arrow gives the spectral range used to compute the  $S_e$  matrices for HCN ( $C_2H_2$ ). (Middle) Contributions of climatological background levels of HCN and  $C_2H_2$ . (Bottom) Contribution of  $CO_2$  (red line),  $O_3$  (green line) and  $H_2O$  (blue line) to a simulated spectrum for background concentrations. Calculations have been made for the US Standard Atmosphere (US Government Printing Office, 1976) with  $CO_2$  concentrations scaled to 390 ppmv.

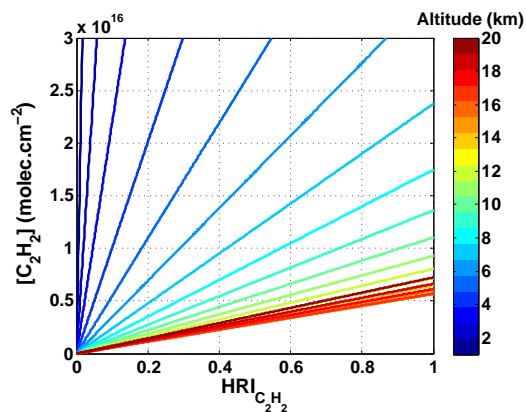
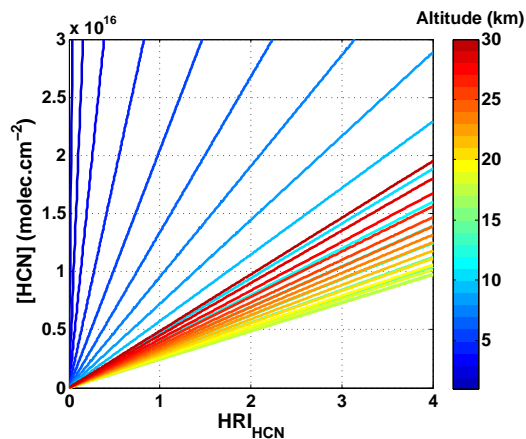


**Figure 2.** Variations of the HRI with HCN (top) and  $C_2H_2$  (bottom) column ( $\text{molec cm}^{-2}$ ) integrated over the 1 km-thick polluted layer in a standard modeled subtropical atmosphere from forward model simulations. The colorscale gives the altitude of the polluted layer.

Global measurements of HCN and  $C_2H_2$  from IASI

V. Dufлот et al.

Title Page

Abstract

Introduction

Conclusions

References

Tables

Figures

◀

▶

◀

▶

Back

Close

Full Screen / Esc

Printer-friendly Version

Interactive Discussion



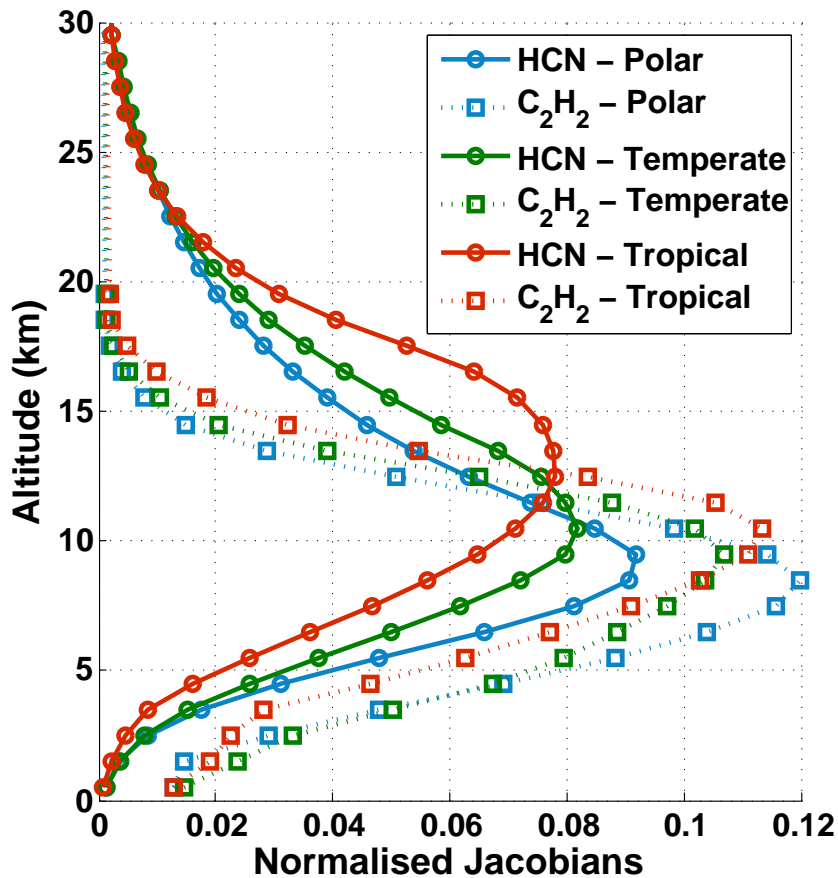


**Figure 3.** Normalised Jacobians of the forward model implemented in *Atmosphit* for HCN (solid lines) and  $C_2H_2$  (dotted lines) and for the standard modeled polar (blue lines), temperate (green lines) and subtropical (red lines) atmospheres. These are averaged Jacobians over the spectral ranges  $645\text{--}800\text{ cm}^{-1}$  for HCN and  $645\text{--}845\text{ cm}^{-1}$  for  $C_2H_2$ .

Global measurements of HCN and  $C_2H_2$  from IASI

V. Dufлот et al.

Title Page	
Abstract	Introduction
Conclusions	References
Tables	Figures
◀	▶
◀	▶
Back	Close
Full Screen / Esc	
Printer-friendly Version	
Interactive Discussion	



Global measurements of HCN and C<sub>2</sub>H<sub>2</sub> from IASI

V. Dufлот et al.

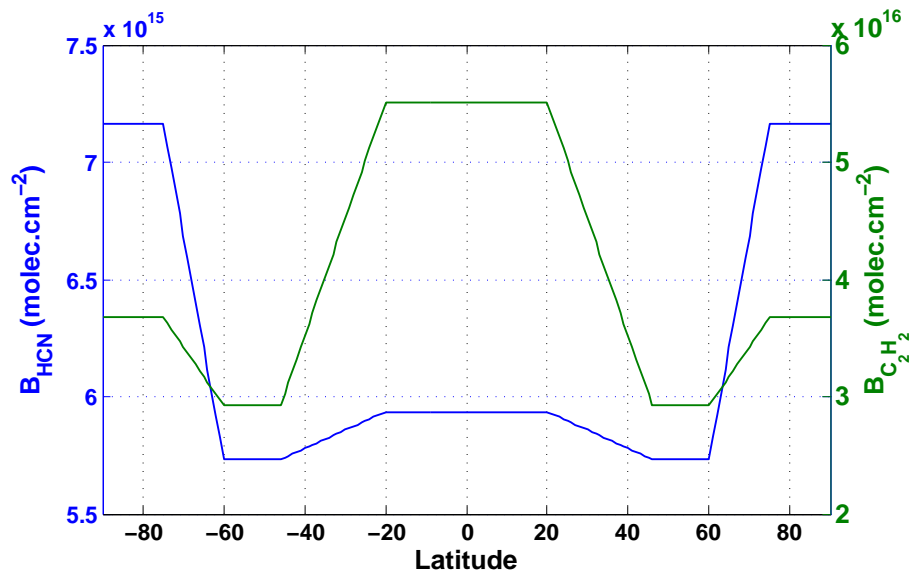


**Figure 4.** Values of  $B_{\text{HCN}}$  (blue) and  $B_{\text{C}_2\text{H}_2}$  (green) as a function of the latitude.

[Title Page](#)[Abstract](#)[Introduction](#)[Conclusions](#)[References](#)[Tables](#)[Figures](#)[◀](#)[▶](#)[◀](#)[▶](#)[Back](#)[Close](#)[Full Screen / Esc](#)[Printer-friendly Version](#)[Interactive Discussion](#)

## Global measurements of HCN and C<sub>2</sub>H<sub>2</sub> from IASI

V. Dufлот et al.

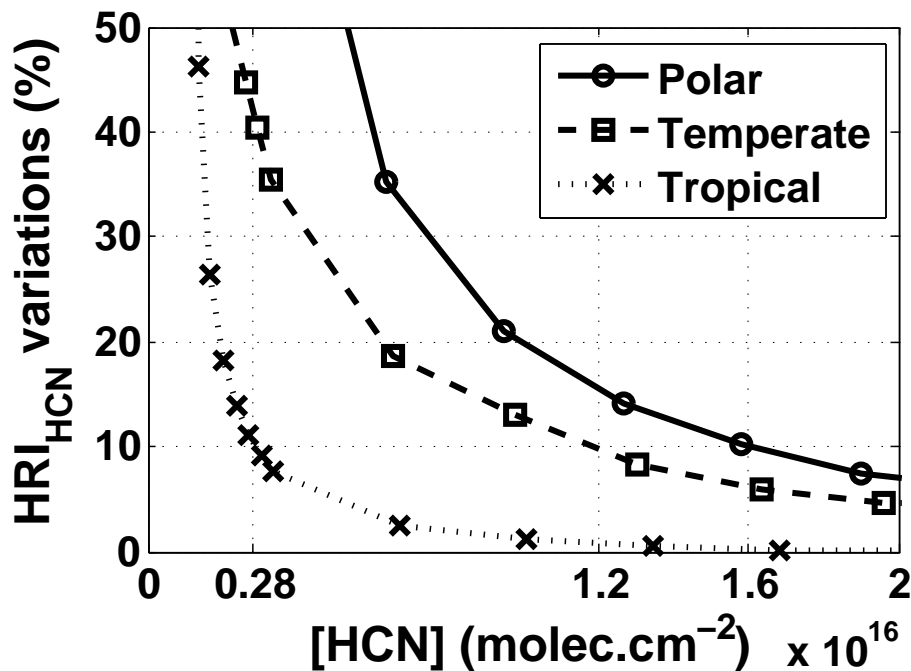


**Figure 5.** Variation of  $\text{HRI}_{\text{HCN}}$  caused by a TC equal to  $\pm 10$  K for the polar (solid line and circles), temperate (dashed line and squares) and tropical (dotted line and crosses) atmospheres.

Title Page

Abstract

Introduction

Conclusions

References

Tables

Figures

◀

▶

◀

▶

Back

Close

Full Screen / Esc

Printer-friendly Version

Interactive Discussion



## Global measurements of HCN and C<sub>2</sub>H<sub>2</sub> from IASI

V. Dufлот et al.

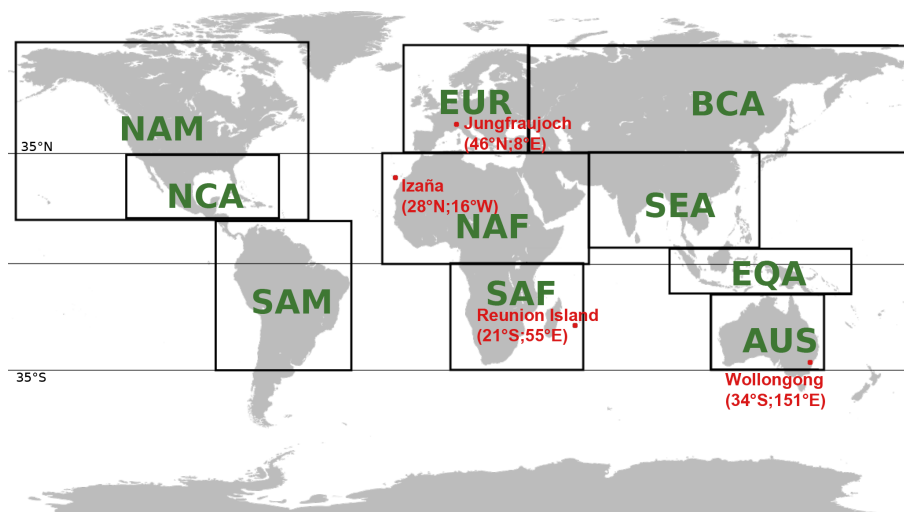


**Figure 6.** Locations of the 4 ground-based FTIR measurements sites (Jungfrauoch, Izaña, Reunion Island and Wollongong) and map of the 10 regions used in this study: NAM: Northern America, NCA: North Central America, SAM: South America, EUR: Europe, NAF: Northern Africa, SAF: Southern Africa, BCA: Boreal Central Asia, SEA: South East Asia, EQA: Equatorial Asia, AUS: Australia.

Title Page

Abstract

Introduction

Conclusions

References

Tables

Figures

◀

▶

◀

▶

Back

Close

Full Screen / Esc

Printer-friendly Version

Interactive Discussion



Global measurements of HCN and C<sub>2</sub>H<sub>2</sub> from IASI

V. Dufлот et al.

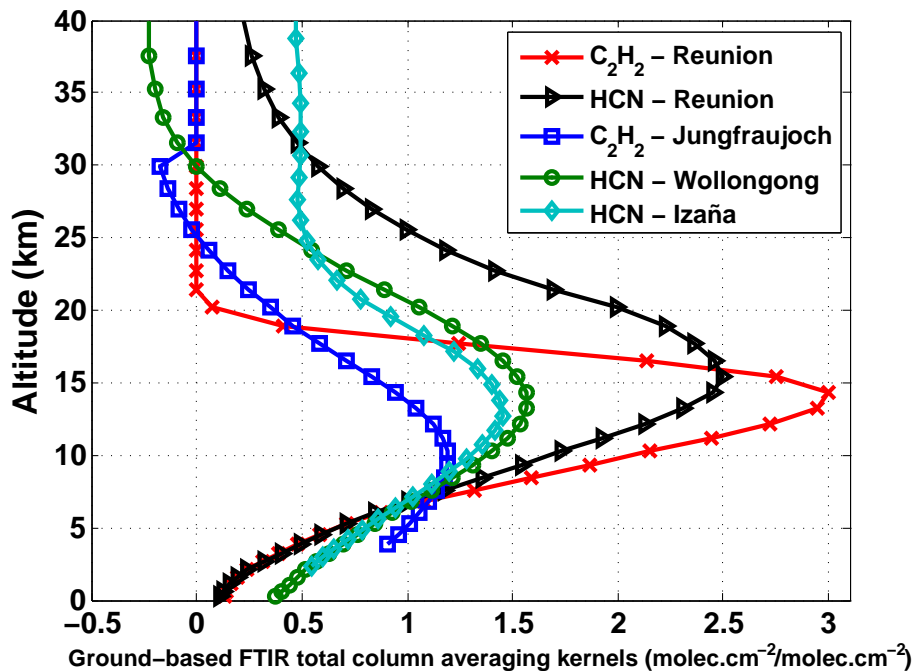


**Figure 7.** Total column averaging kernels of ground-based FTIR in  $\text{molec cm}^{-2}/\text{molec cm}^{-2}$  for C<sub>2</sub>H<sub>2</sub> at Reunion Island (red stars and line), HCN at Reunion Island (black circles and line), HCN at Wollongong (green dots and line), HCN at Izaña (light blue diamonds and line) and C<sub>2</sub>H<sub>2</sub> at Jungfrauoch (blue squares and line).

[Title Page](#)[Abstract](#)[Introduction](#)[Conclusions](#)[References](#)[Tables](#)[Figures](#)[◀](#)[▶](#)[◀](#)[▶](#)[Back](#)[Close](#)[Full Screen / Esc](#)[Printer-friendly Version](#)[Interactive Discussion](#)

Global measurements of HCN and C<sub>2</sub>H<sub>2</sub> from IASI

V. Dufлот et al.

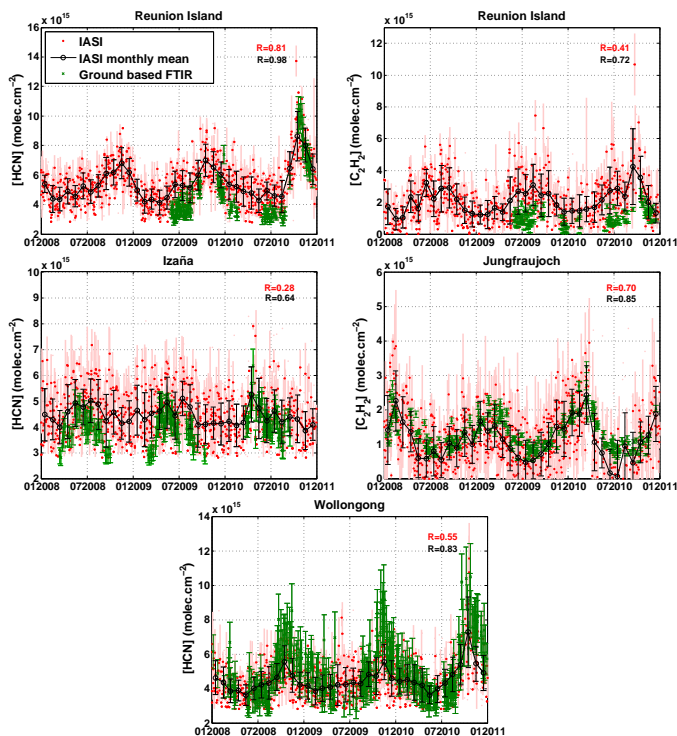


**Figure 8.** Time series of HCN (left panel) and C<sub>2</sub>H<sub>2</sub> (right panel) measurements for Reunion Island (HCN and C<sub>2</sub>H<sub>2</sub>), Wollongong (HCN only), Izaña (HCN only), and Jungfraujoeh (C<sub>2</sub>H<sub>2</sub> only). IASI measurements are shown as daily and 1° × 1° means (red dots) with associated SDs (light red lines), and as monthly and 1° × 1° means (black circles and line) with associated SD (vertical black lines). Ground-based FTIR measurements are shown as daily means with associated total error by green crosses and lines. Correlation coefficients are given on each plot for daily means in red and for monthly means in black.



## Global measurements of HCN and C<sub>2</sub>H<sub>2</sub> from IASI

V. Dufлот et al.

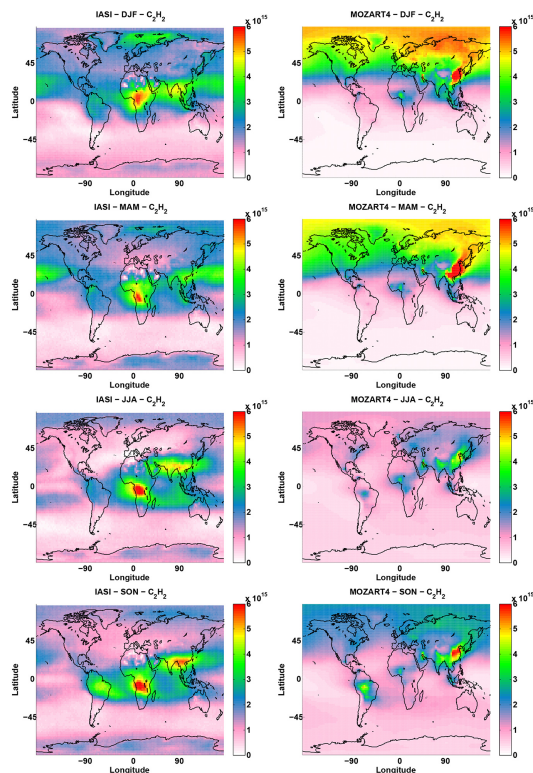


**Figure 9.** Seasonal distribution of the C<sub>2</sub>H<sub>2</sub> total column (in molec cm<sup>-2</sup>) as measured by IASI (left panel) and simulated by MOZART-4 (right panel) averaged over the years 2008 to 2010. The IASI global distributions are given with the same horizontal resolution as MOZART-4 (1.875° latitude × 2.5° longitude). DJF = December–January–February, MAM = March–April–May, JJA = June–July–August, SON = September–October–November.

[Title Page](#)
[Abstract](#)
[Introduction](#)
[Conclusions](#)
[References](#)
[Tables](#)
[Figures](#)
[Back](#)
[Close](#)
[Full Screen / Esc](#)
[Printer-friendly Version](#)
[Interactive Discussion](#)

Global measurements of HCN and C<sub>2</sub>H<sub>2</sub> from IASI

V. Dufлот et al.

Title Page

Abstract

Introduction

Conclusions

References

Tables

Figures



Back

Close

Full Screen / Esc

Printer-friendly Version

Interactive Discussion

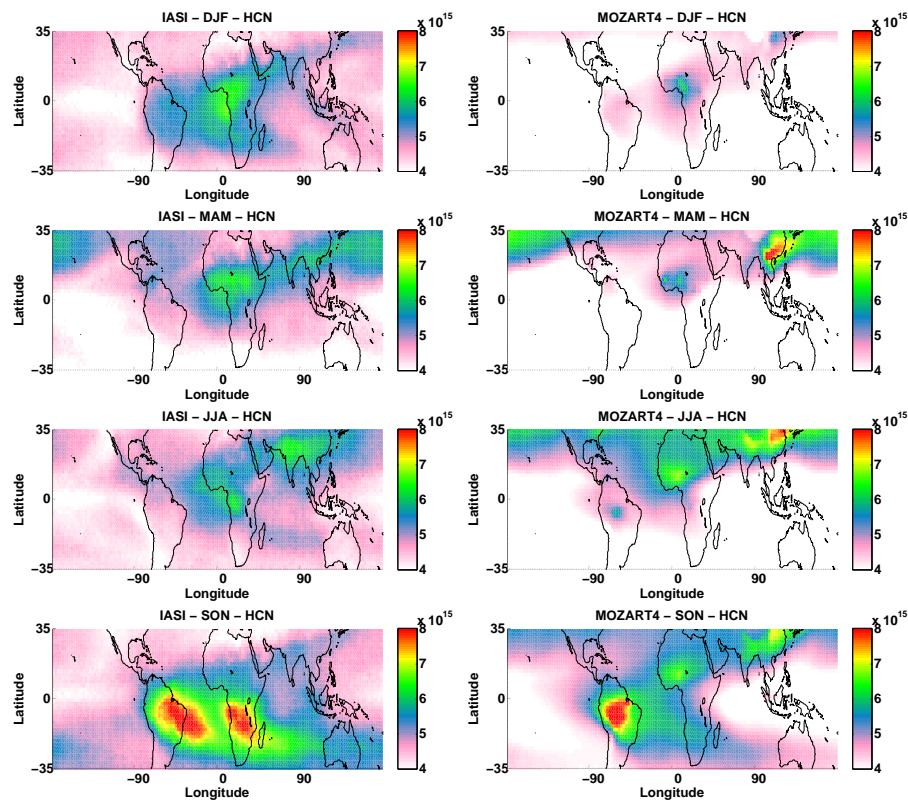


Figure 10. Same as Fig. 9 for HCN.

## Global measurements of HCN and C<sub>2</sub>H<sub>2</sub> from IASI

V. Dufлот et al.

Title Page

Abstract

Introduction

Conclusions

References

Tables

Figures

◀

▶

◀

▶

Back

Close

Full Screen / Esc

Printer-friendly Version

Interactive Discussion

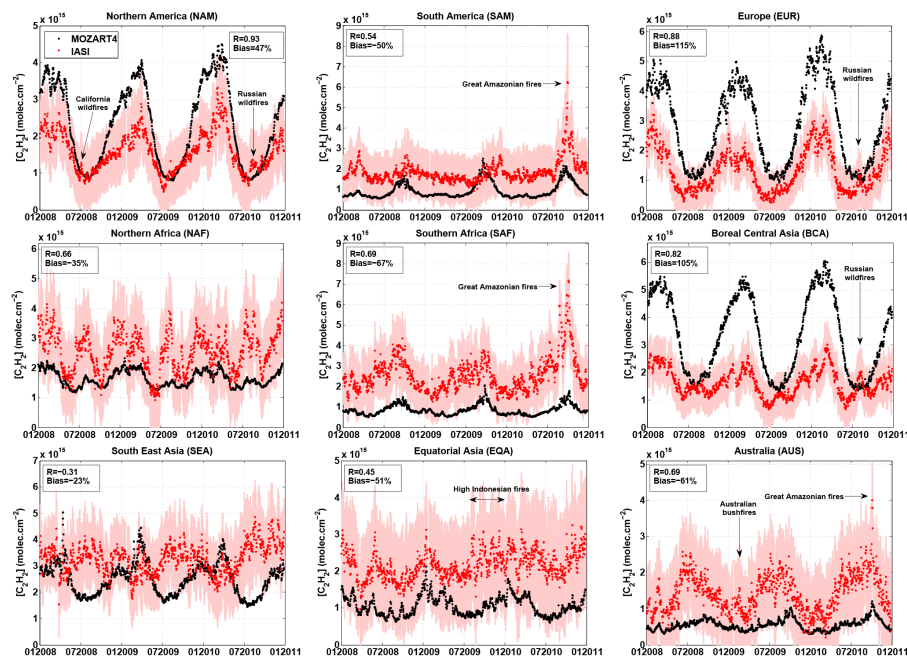


**Figure 11.** Evolution with time of the mean C<sub>2</sub>H<sub>2</sub> total column (in molec cm<sup>-2</sup>) over the zones defined in Fig. 6 as measured by IASI (red dots) with associated SD (light red lines), and as simulated by MOZART-4 (black dots). Correlation coefficients ( $R$ ) and biases (Bias) between IASI and MOZART-4 are given on each plot for daily means.

Global measurements of HCN and C<sub>2</sub>H<sub>2</sub> from IASI

V. Dufлот et al.

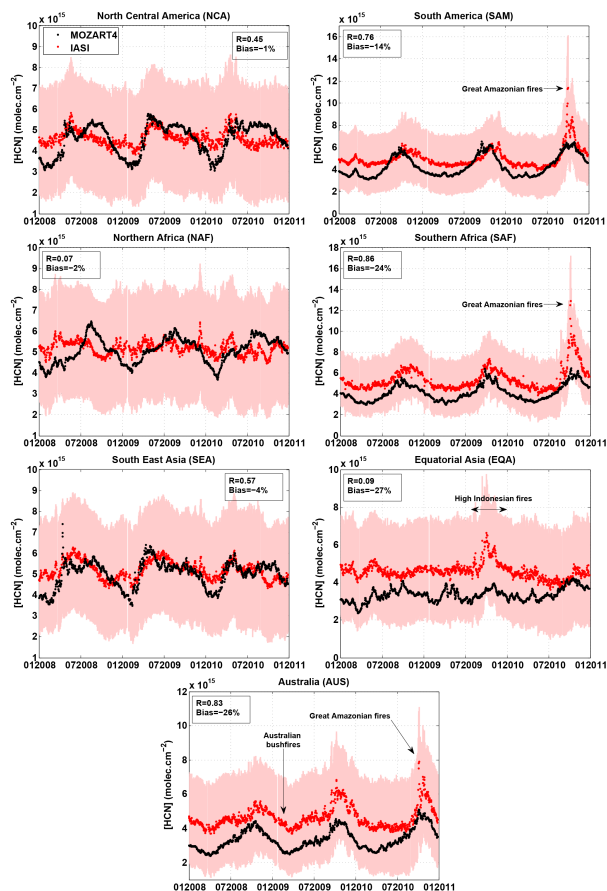


Figure 12. Same as Fig. 11 for HCN.

Title Page

Abstract Introduction

Conclusions References

Tables Figures

◀ ▶

◀ ▶

Back Close

Full Screen / Esc

Printer-friendly Version

Interactive Discussion



Global measurements of HCN and C<sub>2</sub>H<sub>2</sub> from IASI

V. Dufлот et al.

Title Page

Abstract

Introduction

Conclusions

References

Tables

Figures

◀

▶

◀

▶

Back

Close

Full Screen / Esc

Printer-friendly Version

Interactive Discussion

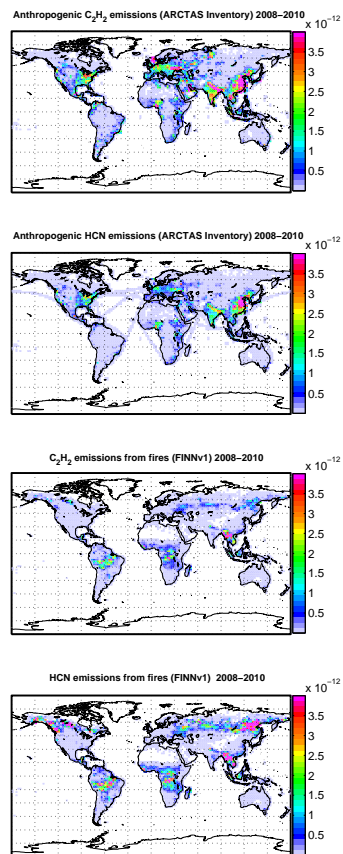


**Figure 13.** C<sub>2</sub>H<sub>2</sub> and HCN surface emission fluxes ( $\text{kg m}^{-2} \text{s}^{-1}$ ) averaged over the period 2008–2010 from the anthropogenic and fire emissions inventories used in MOZART-4.